JOURNAL OF GEOPHYSICAL RESEARCH, VOL. 104, NO. D6, PAGES 6583-6602, MARCH 27, 1999

Simulating the water balance of the Aral Sea with a coupled regional climate-lake model

Eric E. Small[1] and Lisa Cirbus Sloan

Earth Sciences Department, University of California Santa Cruz

Steven Hostetler

U.S. Geological Survey, Corvallis, Oregon

Filippo Giorgi

National Center for Atmospheric Research, Boulder, Colorado

Abstract. Before coupled atmosphere-lake models can be used to study the response of large lake systems to climatic forcings, we must first evaluate how well they simulate the water balance and associated lake atmosphere interactions under present-day conditions. We evaluate the hydrology simulated by a lake model coupled to NCAR's regional climate model (RegCM2) in a study of the Aral Sea. The meteorological variables that are input to the lake model are simulated well by RegCM2. Simulated surface air temperatures closely match observed values, except during spring and fall when the simulated temperatures are too cold. The magnitude of precipitation is too high in the region surrounding the Aral Sea during summer and fall. On a yearly basis, RegCM2 produces a reasonable amount of runoff throughout the drainage basin. The lake model coupled to RegCM2 accurately simulates Aral Sea surface temperatures (SSTs). The lake model also simulates observed mid-winter ice fraction well, although the onset of ice growth occurs too late in the year and the ice melts too rapidly in the spring. The simulated annual evaporation from the Aral Sea is consistent with observed estimates; however, the simulated evaporation is greater than observed during summer and less than observed during winter. In a "stand-alone" lake model simulation, the simulated Aral Sea hydrology does not match observations as closely as in the coupled model experiment. These results suggest that a stand-alone lake model would not accurately simulate the hydrologic response of the Aral Sea to various forcings.

1. Introduction

The hydrologic budget of a lake reflects interactions between processes acting on many spatial and temporal scales. Understanding the interactions between these processes and identifying which processes exert the greatest influence on the water balance of lakes is essential for interpreting the detailed record of terrestrial paleoclimate change preserved in lacustrine sediments. In addition, understanding lake-atmosphere interactions is useful for anticipating the response of lake systems to various anthropogenic forcings, including enhanced atmospheric greenhouse gases and decreased lake inflow resulting from diversions of natural river water.

Observational studies of lake systems provide important information about lake hydrology [e.g., *Changnon and Jones*, 1972]. However, a modeling approach is useful for understanding interactions between lake and atmosphere processes and to assess how lake systems may respond to various forcings. Physically based models are only useful if they accurately portray the various climatic and hydrologic processes that influence lake systems. The primary goal of this study is to assess if a lake model coupled to a regional climate model can accurately simulate the hydrology of a large lake system, including lake surface temperatures, ice cover, and the various components of the water balance of a lake. Our secondary goal is to examine how lake-atmosphere interactions influence the hydrology of a large lake system. If lake-atmosphere interactions exert only a weak influence on the hydrology of large lakes, then a coupled atmosphere-lake model may not be necessary in climate and hydrology change studies. We address these two issues by analyzing a 5 year coupled regional climate/lake model simulation of the present-day climate and hydrology of the Aral Sea in central Asia (Figure 1), produced with the National Center for Atmospheric Research (NCAR) regional climate model (RegCM2).

In many previous studies of lake-atmosphere systems, models have been used that do not represent the interactions between surface water and atmosphere. For example, limited-area atmospheric models have been used to examine the influence of lakes on the development of individual storms [e.g., *Hjelmfelt*, 1990]. In these studies, the lake surface temperature and ice cover are typically prescribed, which prohibits lake-atmosphere interactions from influencing the outcome of the simulation. Studies have also been completed

[1]Now at Department of Earth and Environmental Science, New Mexico Tech, Socorro, NM.

Paper number 98JD02348.
0148-0227/99/98JD-02348$09.00

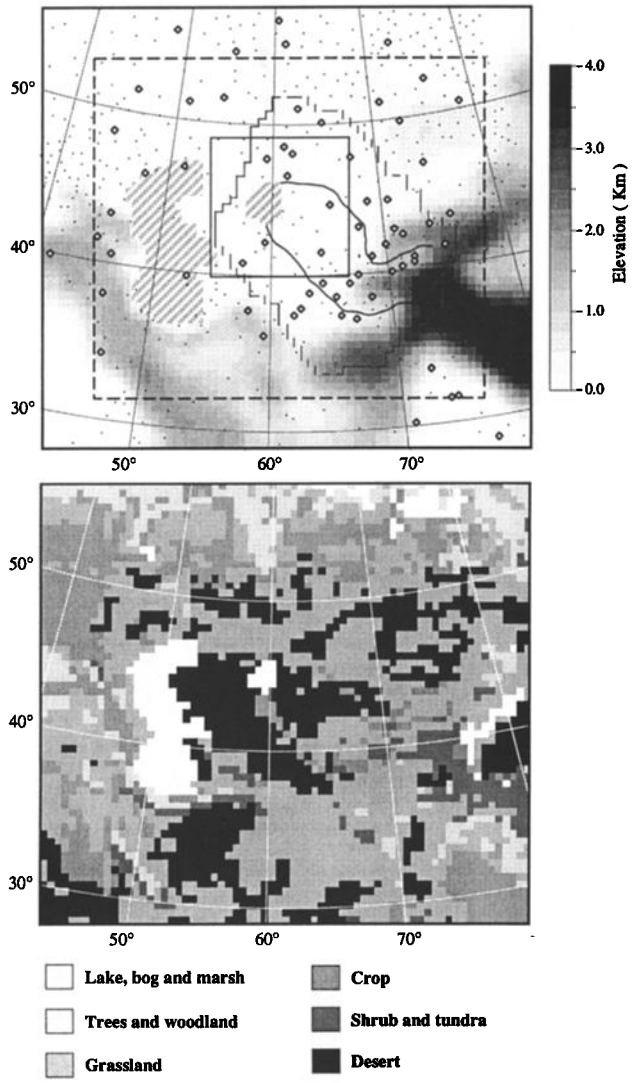

Figure 1. Numbers on outside of maps indicate degrees north latitude and degrees east longitude. (top) Shading depicts surface elevation. The Caspian (left) and Aral Seas (center) are hatched The irregularly shaped polygon shows the Aral Sea drainage basin boundary and the two curves ending at the Aral Sea represent the Amu Darya (south) and Syr Darya (north). The small square in the center of the domain shows the near Aral region. Dots show location of Climate Analysis Center (CAC) meteorological stations from which temperature measurements were used. The larger open symbols show locations of CAC stations from which precipitation and temperature data were used. The dashed rectangle shows the inner edge of the buffer zone throughout which boundary conditions are applied. (bottom) Biosphere-atmosphere transfer scheme (BATS) land cover categories for the model domain. Not all 14 BATS categories are shaded differently. Instead, like categories (e.g., tall and short grass) have been shaded similarly.

in which a lake model is forced by meteorological inputs [e.g., *Hostetler and Giorgi*, 1995]. Again, feedbacks between the lake and the atmosphere are not represented in these simulations.

Models have also been used in which the interactions between surface water and atmosphere are explicitly represented. *Bonan* [1995] examined the effects of representing inland water surfaces in a global climate model simulation by calculating surface fluxes separately for the land and water fraction of each grid cell. *Coe and Bonan* [1997] used this method to examine the impact of expanded surface waters on the summer monsoon of north Africa at 6000 years before present. Also using a global model, *Lofgren* [1997] examined the simulated climatological effects of the Great Lakes by comparing experiments with and without these inland water bodies. Not all important lake and atmosphere processes are well represented at the resolution of a global model [*Lofgren*, 1997]. An alternative approach is to use a relatively high-resolution regional climate model that resolves mesoscale forcings on the climate system [*Giorgi and Mearns*, 1991]. *Hostetler et al.* [1994] used the NCAR RegCM coupled to a lake model to identify feedbacks that could explain the anomalously large response of Lake Bonneville to the Pleistocene pluvial climate of the Great Basin. *Bates et al.* [1995] used the same model to simulate the present-day climate of the Great Lakes region.

Even though coupled atmosphere-lake models have been used in previous studies, simulated lake water budgets have not been compared to observations, or observations were not available. Therefore it is unknown how accurately coupled models simulate the hydrologic budgets of lakes. In addition, it has not been established that coupled models can successfully reproduce lake surface temperature and ice cover, both of which strongly influence lake-atmosphere interactions. *Bates et al.* [1995] presented a limited comparison between simulated and observed lake surface temperatures and ice cover; however, there were large model temperature biases during most of the year, and substantial differences existed between the simulated and the observed ice cover. Previous studies have also failed to demonstrate that representation of lake-atmosphere feedbacks improves the simulation of lake hydrologic processes, compared to an experiment in which these interactions are not included. We examine this issue by comparing results from a coupled model simulation to those from a "stand-alone" lake model experiment in which lake-atmosphere interactions are excluded.

The work presented here is part of a larger effort to study climatic and hydrologic changes associated with anthropogenic desiccation of the Aral Sea. In 1960 the surface area of the Aral Sea was ~70,000 km^2, making it the fourth largest inland water body on Earth by surface area (Table 1) [*Micklin*, 1988]. The surface area of the Aral Sea has decreased by ~50% since this time because river inflow to the Aral Sea was severely reduced as the result of intense irrigation in the Aral Sea drainage basin. By simulating this large land surface change with the RegCM2-lake modeling system, we intend to differentiate between climatic and hydrologic changes associated with Aral Sea desiccation and those that are due to larger-scale forcings. The results from this effort will be reported in a forthcoming paper.

In the present paper, we first describe the regional climate and lake models and details of the model experiments (section 2). We then describe the various climatic and hydrologic observations used to assess model performance (section 3). This is followed by a comparison of the observed and simulated surface air temperature and precipitation (section 4). We then assess how well the coupled RegCM2-lake model simulates the observed sea surface temperatures, ice cover, and water balance of the Aral Sea (section 5). Finally, we evaluate

Table 1. Observed Characteristics of the Aral Sea in 1960 and 1990 and Corresponding Values Used in the Coupled RegCM2- Lake Model Control Simulation

	1960	1990	1990
	Observed	Observed	Simulated
Surface area (10^3 km^2)	65-75	37	35
Mean depth (m)	15	8	10
Volume (km^3)	1100	300	350
Salinity (ppt)	10	33	33

if lake-atmosphere interactions exert a strong influence on the water balance of the Aral, and if a coupled model approach is necessary in climatic and hydrologic change studies of large lake systems (section 6).

2. Experimental Design

2.1. Regional Climate Model

In this study, we use a version of NCAR's regional climate model, RegCM2. Because this model is described in detail elsewhere [*Giorgi et al.*, 1993a,b], we include only a brief description here. The NCAR RegCM was originally developed by *Dickinson et al.* [1989], *Giorgi and Bates* [1989], and *Giorgi* [1990]. It is an augmented version of the NCAR/Pennsylvania State University mesoscale model MM4 [*Anthes et al.*, 1987]. MM4 is a primitive equation, σ vertical coordinate, grid point limited-area model with compressibility and hydrostatic balance. Some of the physics parameterizations that were added to MM4 to improve its suitability for climate studies include (1) the convection parameterizations of *Grell* [1993], (2) *Holtslag et al.* [1990] nonlocal formulation of vertical transport in the planetary boundary layer, (3) the NCAR CCM2 radiative transfer package, which explicitly accounts for the effects of CO_2, O_3, H_2O, O_2, and clouds [*Briegleb*, 1992], (4) a simplified explicit cloud water scheme which prognostically calculates precipitation and cloud water for radiation calculations [*Giorgi and Shields*, this issue], and (5) the biosphere-atmosphere transfer scheme (BATS) surface physics package [*Dickinson et al.*, 1993].

2.2. Lake Model

To account for the surface fluxes of heat, moisture, and momentum from the Aral and Caspian Seas, we use a lake model that is interactively coupled to RegCM2 [*Hostetler et al.*, 1993]. This model is a modified version of *Hostetler and Bartlein*'s [1990] one-dimensional, energy balance lake model (Figure 2). In this study, the lake model is used to compute (1) Aral sea surface temperatures (SSTs), (2) Aral and Caspian ice thickness and ice/snow surface temperatures, and (3) surface fluxes from both water bodies. We prescribe Caspian SSTs (discussed below) because a one-dimensional heat transfer approach is inadequate to represent the complex circulation in the Caspian. When the Caspian SST data indicate water is at or below the freezing point, ice thickness and surface temperature are calculated using the ice scheme of the lake model.

2.2.1. Vertical heat transfer. Energy is transferred vertically between lake model layers (dz = 1 m) by eddy and molecular diffusion and by convective mixing. The eddy diffusion component represents turbulent vertical mixing which results from vertical gradients in the velocity of wind-induced currents [*Henderson-Sellers*, 1985]. Convective mixing removes density instabilities within the lake column which are generated by surface heating and cooling. The convective mixing is completed in a way that conserves the total energy of the mixed portion of the water column.

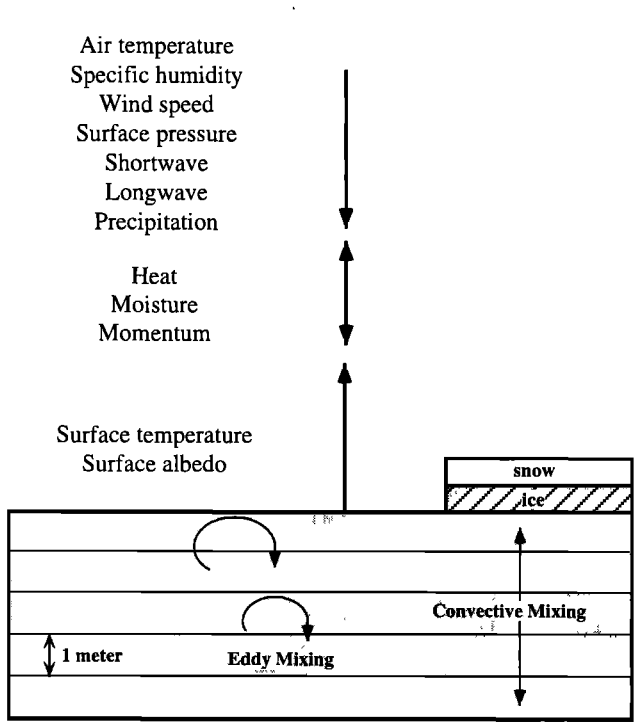

Figure 2. Lake model schematic. Fluxes of heat, moisture, and momentum are calculated based on meteorological inputs and the lake surface temperature and albedo. Heat is transferred vertically between lake model layers by eddy and convective mixing. Ice and snow may cover part or all of the lake surface.

We use the parameterization of *Henderson-Sellers* [1985] to calculate the eddy diffusivity at each model layer. This parameterization includes a gradient Richardson number adjustment to account for nonneutral conditions. This adjustment results in reduced eddy diffusion under stable conditions, which reduces vertical heat transfer across the simulated thermocline. Temperature (T) changes are the product of the sum of the eddy (k_e) and molecular (k_m) diffusivities and the vertical curvature of the temperature profile.

$$\frac{\partial T}{\partial t} = (k_e + k_m)\frac{\partial^2 T}{\partial z^2} \quad (1)$$

Typically, eddy diffusivity is much greater than molecular diffusivity ($k_m = 1.39 \times 10^{-7}$ m^2 s^{-1}) except under ice and at the deepest points within lakes. In previous applications of this model [e.g., *Bates et al.*, 1995], eddy diffusivities were frequently lowered to maintain numerical stability. To avoid this problem, we have implemented a Crank-Nicholson numerical solution. This modification allows the full range of values calculated from the *Henderson-Sellers* [1985] parameterization to be used. This results in deeper and more rapid mixing of heat and improves the simulation of lake surface temperatures throughout the year.

2.2.2. Surface energy balance. The surface energy balance calculations differ from those of *Hostetler and Bartlein* [1990]. We use BATS version 1e parameterizations to calculate moisture and sensible heat fluxes from the lake surface [*Dickinson et al.*, 1993]. In this bulk transfer formulation the moisture flux (F_q) or evaporation from the surface is proportional to the surface-air difference in specific humidity (q_s-q_a):

$$F_q = \rho_a C_D V_a (q_s - q_a) \quad (2)$$

where the subscripts s and a refer to surface and air, respectively; ρ_a is the density of air; and V_a is wind speed. The surface specific humidity is equal to the saturation specific humidity of water at the surface temperature. The momentum drag coefficient C_D is a function of (1) the neutral drag coefficient, which depends on roughness length; and (2) the surface bulk Richardson number, which depends on the wind speed and the near-surface temperature gradient. Thus the stability of the boundary layer affects evaporation, with unstable conditions leading to greater evaporation.

The calculation of the sensible heat flux (F_s) is similar to that of the latent heat flux:

$$F_s = \rho_a C_p C_D V_a (T_s - T_a) \quad (3)$$

C_p is the specific heat of air. Because of the Richardson number dependence on (T_s-T_a) in the calculation of the momentum drag coefficient, sensible heating is non-linearly related to the surface-air difference in temperature.

When the lake surface is ice free, the lake surface albedo is calculated as a function of solar zenith angle [*Henderson-Sellers*, 1986]. The surface albedo is ~0.07 when the solar zenith angle is < ~75° and increases rapidly for higher zenith angles to ~0.20 when the Sun is on the horizon. Forty percent of the surface-absorbed shortwave radiation is absorbed within the top 0.6 m of the lake [*Henderson-Sellers*, 1986]. Absorption of the remaining shortwave radiation decreases exponentially with depth, with a scale length constrained by water transparency (discussed below). Longwave radiation off the lake surface is calculated according to the Stefan-Boltzmann law.

2.2.3. Salinity effects. Uniform salinity is prescribed throughout the water column and is held constant throughout the simulation examined here. The salinity of the Caspian and Aral Seas were set at observed values. The effect of salinity on the density, specific heat, and freezing point of water are calculated according to *Gill* [1982]. We use empirical relationships [*Dickinson et al.*, 1965] to calculate changes in the saturation vapor pressure of water due to salinity.

2.2.4. Lake ice and snow cover. We have implemented a partial ice cover scheme to represent the different heat and moisture exchanges between open water and ice surfaces and the atmosphere [*Patterson and Hamblin*, 1988]. Ice growth occurs in both the open water and the ice covered fractions of a grid cell when the water temperature is at the (salinity dependent) freezing point and the surface energy balance is negative. Ice growth does not change the salinity of the underlying water. A fraction of the grid cell remains open water until enough ice has grown to cover the entire grid cell at a prescribed minimum thickness: 10 cm in the simulation discussed here. The surface energy balance of lake ice and overlying snow are calculated according to *Patterson and Hamblin* [1988]. Solar radiation that penetrates the lake ice is absorbed by the underlying water column as described above. At the end of each lake time step, the temperature profiles beneath open water and ice are averaged at each depth.

2.2.5. Lake-atmosphere interactions. The lake model is interactively linked to RegCM2. At each lake model time step (30 minutes), air temperature, surface pressure, wind speed, specific humidity, precipitation, and downward short and long wave radiation from the lowest atmospheric model level are passed to the lake model (Figure 2). Based on these meteorological inputs and the lake surface temperature and albedo, the lake model calculates the lake-atmosphere exchanges of moisture, heat, and momentum. The lake surface energy balance is then calculated from these quantities. The lake surface temperature and the temperature profile within the lake are adjusted based on the surface energy balance. The updated surface temperature and albedo are then ready to be used in the next timestep.

There is a single lake model vertical column for each RegCM2 grid cell in which the BATS land cover category is specified as "lake". No transfer of heat or other quantities is allowed between adjacent lake points.

2.2.6. "Stand-alone" configuration. We also use the lake model in a stand-alone configuration. With this setup, meteorological inputs derived from RegCM2 output are passed to the lake model at each time step. The lake model then calculates the surface fluxes and adjusts the lake temperature and ice in the same way as described above for the coupled-model configuration. In the stand-alone configuration the updated surface temperature and ice cover do not influence the meteorological inputs at the next time step.

2.3. Model Domain

The model domain used here has a resolution of 50 km, covers a 3400 x 3100 km^2 area, and includes the entire Aral Sea drainage basin (ASDB) (Figure 1). The ASDB shown in Figure 1 was topographically defined at 50 km resolution: water falling on grid cells within the drainage basin boundary flow to the Aral Sea. Defined in this way, the ASDB covers an

area of ~1.9 x 10^6 km^2. Most of the low-elevation (< 250 m) areas within the basin are locally internally drained and do not contribute runoff to the Aral. Nearly all of the runoff that feeds the Aral Sea comes from the Pamir and Tien Shan Mountains in the southeastern corner of the drainage basin. Two rivers, the Amu Darya and Syr Darya, transport runoff ~2000 km from the mountains to the Aral Sea.

BATS vegetation/land cover categories (Figure 1) were set according to Olsen's 30-minute global ecosystem data set available in the NCAR data archive. The only areas of surface water within the domain are the Caspian and Aral Seas as well as some wetlands along the northern and eastern boundaries. The Aral Sea is surrounded by extensive deserts, except on the northern side where grasslands predominate. Cropland is present along the Amu Darya and throughout the Amu Darya delta.

To assess how well RegCM2 simulates precipitation and temperature, both of which impose a strong influence on the water balance of the Aral Sea, we compare observations and model output averaged over two areas: (1) the ASDB and (2) a low-elevation area in the center of the domain, which we refer to as the "near-Aral" region. The near-Aral region is 1000 km on a side, and is intended to have a climate that is representative of that near the Aral Sea.

2.4. Experimental Design

We integrated RegCM2 for two continuous ~5.5 year periods, from June 1, 1987 to January 1, 1993. In the first experiment the Aral Sea is represented by the lake model which is interactively coupled to RegCM2. The surface area, depth, and salinity of the Aral Sea were set to 1990 observed values (Table 1). This simulation is referred to as the coupled model "control" simulation. We test RegCM2's ability to simulate the present-day water balance of the Aral by comparing output from this simulation with temporally corresponding observations. In the second experiment, the Aral Sea was removed and replaced by desert. This simulation is referred to as the "no-lake" experiment. Desert was used to replace the Aral because it is the natural land surface type that would exist in the absence of the sea (Figure 1). The environmental change that has accompanied desiccation since 1960 indicates that this is the case [*Micklin*, 1988]. We use output from this simulation to construct the meteorological inputs for a stand-alone lake simulation, in which we examine if lake-atmosphere interactions are important to the accurate simulation of the water balance of the Aral Sea.

The Aral Sea covers 14 model grid cells in the control simulation (Table 1). This results in a surface area of 35,000 km^2, which is similar to the 1990 observed value of 37,000 km^2. The depth at each model grid cell was set according to the grid cell mean depth in 1990 determined from an ~1 km resolution bathymetric map of the Aral Sea (R. Ressl, personal communication, 1996). Salinity was prescribed at 33 ppt, again according to the 1990 observed value. The exponential length scale η over which shortwave radiation is absorbed was varied spatially according to observed Secchi Disk depth measurements [*Bortnik*, 1990] and empirical relationships between Secchi Disk measurements and η [*Graham*, 1966]. At each location, η is constant throughout the year.

The time-dependent lateral boundary conditions were the same for both simulations. Wind, temperature, water vapor, and surface pressure were taken from 12 hourly European Centre for Medium-Range Weather Forecasts (ECMWF) analyses on a T42 spectral grid [*Trenberth*, 1992]. These boundary conditions were applied over a 400 km buffer zone along the lateral boundaries of the domain (Figure 1). This was done using the relaxation method of *Anthes et al.* [1987] modified by *Giorgi et al.* [1993b].

Time-dependent Caspian SSTs were prescribed according to the Pathfinder AVHRR SST data set, available from the Physical Oceanography Distributed Active Archive Center (PODAAC) at the Jet Propulsion Laboratory. The Pathfinder data used here has a spatial resolution of 50 x 50 km^2 and monthly temporal resolution. When the Pathfinder data indicated sea ice was present in the Caspian, ice thickness and surface temperature were calculated using the ice scheme of the inland water model discussed above. We prescribe Caspian SSTs so that the effects of this lake on the Aral Sea are represented in the simulations. Evaporation from the Caspian likely increases the specific humidity over the Aral, with the greatest change occurring during fall when the Aral is directly downwind of the Caspian, and Caspian SSTs are warm. In addition, the Caspian may also affect the air temperature over the Aral, cooling (warming) the air in spring/summer (fall/winter). During summer a high pressure builds over the Caspian Sea that enhances the northwesterly flow caused by the Azores High [*Lydolph*, 1977]. This increases the northwesterly flow over the western edge of the Aral Sea. Overall, we expect that the effects of the Caspian on the Aral are minor; however, the model experiments discussed here are not designed to address this issue.

In the control simulation, we initialized the lake temperature profile at each lake point by driving the lake model with 6 hourly inputs derived from the International Satellite Land Surface Climatology Project (ISLSCP) data set. The ISLSCP inputs were taken from a point over the Aral Sea and represent a two-year interval (1987-1988). These two years of data were repeatedly input to the lake model until temperature at the deepest lake points stopped changing, which took ~10 years. Temperature profiles from June 1, 1987, were then used to initialize the coupled model. We exclude the first seven months of the coupled simulation (June-December 1987) from all analyses to minimize possible problems associated with model spin-up. This leaves five complete years (1988-1992) for which we compare model output to observations.

3. Observations

3.1. Temperature and Precipitation

We use the Legates and Willmott 0.5° x 0.5° gridded precipitation climatology (LWC) [*Legates and Willmott*, 1990] and the Climate Analysis Center (CAC) monthly data set to evaluate how well RegCM2 simulates precipitation. Both data sets are available in the NCAR data archive. The LWC was constructed using roughly 60 years of monthly station data (1920-1980). On the basis of empirical relationships, rain gauge type, and local climatic conditions, the long-term monthly means from each station were adjusted for losses resulting from wind, gauge wetting, and evaporation from gauges [*Legates and Willmott*, 1990]. We use the spatially varying precipitation correction for each month to estimate biases in the CAC precipitation data set. Monthly precipitation records from many CAC meteorological stations

in central Asia are incomplete. As discussed by Small et al. [this issue], 65 stations with continuous records were chosen for comparison with model output (Figure 1). Thirty two of these stations are within the ASDB. As we found no problems with CAC temperature data, we use all stations (~400) for our analyses (Figure 1). We do not use monthly precipitation or temperature values determined from fewer than 25 daily reports.

3.2. Aral Sea Surface Temperature

We compare simulated Aral sea surface temperatures (SSTs) with both in situ and satellite-derived measurements. The in situ SST measurements were acquired from the State Oceanographic Institute in Russia. These SSTs were measured during a series of seven boat surveys between 1988 and 1992. Each survey includes ~50 observations spread evenly across the Aral. SST observations were recorded at a depth of 0.5 m. No surveys were completed between November and April, except for a single survey in February.

To conduct a more extensive test of model performance, we also use multi channel sea surface temperature (MCSST) data derived from the NOAA advanced very high resolution radiometer (AVHRR) [*McClain*, 1989; *McClain et al.*, 1985]. The AVHRR measures reflected and emitted radiation in four to five wavelength bands. These measurements are converted to SSTs based on a set of calibration coefficients determined from a previous comparison between AVHRR data and buoy-derived SSTs [*McClain*, 1989]. Compared to buoy and boat measurements not included in the calibration, the MCSST observations exhibit a mean cold bias of ~0.35°C with a standard deviation of 0.65°C. The instantaneous AVHRR measurements are combined into 8 day averages, for both daytime and nighttime observations. The version of the data used here has a spatial resolution of ~17 km. MCSST data were not recorded when thick clouds existed over the Aral Sea.

3.3. Aral Sea Water Balance

The rate of change in volume of the Aral Sea (dV/dt = cm^3/month) represents the balance between the volume of runoff into the sea (R = cm^3/month) and the rates of precipitation (P = cm/month) and evaporation (E = cm/month) over the lake's surface area (A_L = cm^2).

$$\frac{dV}{dt} = R + A_L(P\text{-}E) \tag{4}$$

As the groundwater contribution to the Aral's hydrologic budget is estimated to be relatively minor [*Sadov and Krasnikov*, 1987], it is not addressed in this study. Direct measurements of precipitation and evaporation over the Aral Sea do not exist. However, this information is essential to evaluate the simulated water balance of the Aral. We calculate the combined contribution of the two quantities, P-E, as a residual in the above water balance equation.

$$(P\text{-}E) = \frac{(\frac{dV}{dt} - R)}{A_L}\Delta SL - \frac{R}{A_L} \tag{5}$$

Monthly values of P-E averaged over the Aral are determined from a time series of monthly sea level (SL), runoff in the Amu and Syr Darya, and surface area observations. These data were obtained from the Hydrometeorological Institute of the Republic of Uzbekistan.

There are two problems associated with calculating monthly P-E according to equation 5. First, monthly sea level measurements were made at only one or two stations during the period 1988-1992. At a single station, the change between consecutive monthly sea level measurements can be divided into two components: (1) a sea-averaged change which reflects the water balance of the sea; and (2) local deviations from the mean due to wind and spatial variations in surface pressure. In some months, the local deviation may be similar in magnitude to the mean change, introducing a substantial error into the corresponding P-E value. This error will be canceled in subsequent months by errors of opposite sign, as the amplitude of the localized sea level deviation diminishes. Therefore, these errors do not influence P-E values when averaged over periods greater than several months.

The second problem with P-E values determined from equation (5) is that runoff measurements may not accurately represent the amount of water added to the Aral sea by the Amu Darya and Syr Darya. The gauging stations on these two rivers are ~50-100 km upstream from the Aral sea shore. Instead of reaching the Aral, some fraction of the water passing the gauge site may be lost in wetlands or in groundwater. To address this issue, we calculate both a minimum and a maximum P-E estimate for each month. The minimum estimate is based on the assumption that all gauged streamflow reaches the Aral Sea, and the maximum is based on the assumption that none of the gauged runoff contributes to the Aral. In many months these two estimates are very close or identical because flow in the Amu Darya and Syr Darya is often minor due to intense irrigation throughout the ASDB. Actual P-E values are probably closer to the minimum estimate in months with substantial runoff. Temporary storage of runoff in wetlands or near-surface aquifers between the gauging stations and the Aral Sea result in P-E errors for a particular month. These errors are canceled in subsequent months when the stored runoff reaches the Aral. Water losses from evaporation or long-term groundwater storage between gauges and the sea produce errors that accumulate throughout the interval examined in this study. Our maximum and minimum estimates are important to quantify the uncertainty associated with these cumulative errors.

4. Simulated and Observed Temperature and Precipitation

In this section, we compare the surface air temperature and precipitation simulated by the coupled RegCM2-lake modeling system to observations. Air temperature affects the surface energy balance of the Aral and therefore influences the evaporation rate from the sea surface. In addition, air temperature influences evaporation from the land surface, which controls how much precipitation within the ASDB contributes to runoff to the sea. Precipitation contributes to the Aral Sea hydrologic budget through rainfall directly over the Aral and through the generation of runoff throughout the ASDB. The performance of RegCM2 in simulating the mean patterns and annual cycle of precipitation as well as the interannual variability of precipitation are described in detail elsewhere [*Small et al.*, this issue]. A brief description of the precipitation as relevant to the Aral Sea water budget is included here.

4.1. Temperature

Figures 3 and 4 and Table 2 show comparisons between simulated 2 m air temperature and observed air temperature

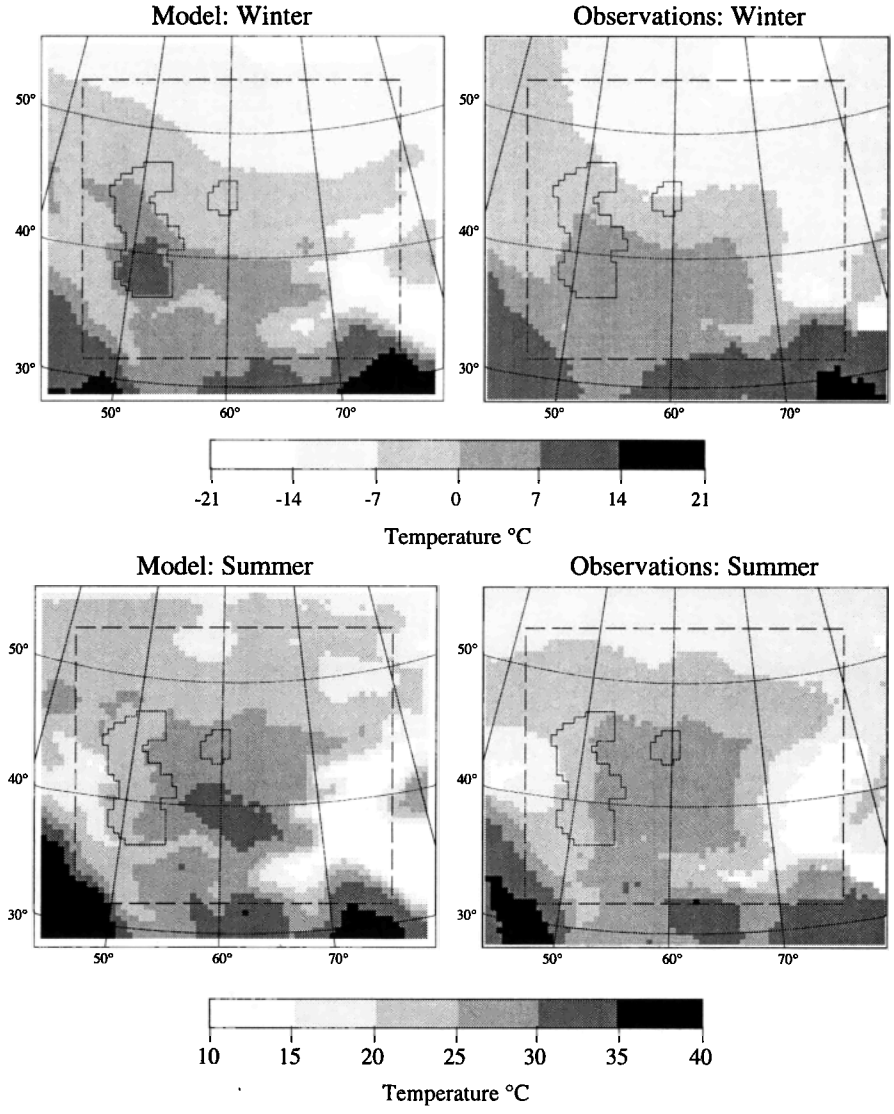

Figure 3. (top) Winter RegCM2 2 m air temperature (left) and CAC monthly average air temperature interpolated onto the model grid (right), averaged for December through February between 1988 and 1992. (bottom) Same for summer temperature, averaged for June - August. The dashed rectangle shows the inner edge of the buffer zone throughout which boundary conditions are applied.

from CAC meteorological stations, averaged monthly and seasonally between 1988 and 1992. We compare observations to BATS 2 m air temperature, which is interpolated between temperatures at the lowest model level (~40 m) and the ground. Whereas monthly mean model temperatures are calculated from hourly BATS values, CAC monthly mean temperatures represent the average of monthly mean maximum and minimum temperatures. This introduces an uncertainty in the model-data comparison. Additional uncertainties result from differences between meteorological station and model grid point elevations [*Giorgi et al.*, 1994; *Jones et al.*, 1995]. To minimize elevation-related errors, we adjust all observed temperatures for the difference between the elevation of the observation station, z_{OBS}, and the model grid cell, z_{RCM}, at that location, using a lapse rate Γ of 6.5°C/km ($t_{adj} = t - (z_{RCM} - z_{OBS}) \times \Gamma$). The elevation adjustment is negligible in the near-Aral region (< 0.1°C), but is large throughout the entire ASDB (1.8°C), owing to the complex topography in the mountainous parts of the drainage basin.

First we evaluate how well the model reproduces the spatial patterns of 2 m air temperature, averaged between 1988 and 1992 for winter and summer (Figure 3). The observations are adjusted for elevation biases and interpolated from ~400 CAC stations (Figure 1) onto the RegCM2 grid. Excluding the boundary regions, the model simulates the observed temperature patterns well. For example, the model reproduces the wintertime NW-SE alignment of isotherms in the NW quadrant of the domain. This pattern is due to the advection of cold air associated with a trough in the 500 mb height field, which leads to relatively cold temperatures in the vicinity of the Aral Sea. In summer, the model reproduces the tongue of cold air from the Black Sea at roughly 40°N, as well as the region of high temperatures over the Aral Sea. Simulated and observed temperature patterns differ in some areas such as the southeastern mountains, primarily where few or no meteorological stations exist and observations have been interpolated across areas with high-temperature gradients. Large differences also exist over the Caspian Sea, where

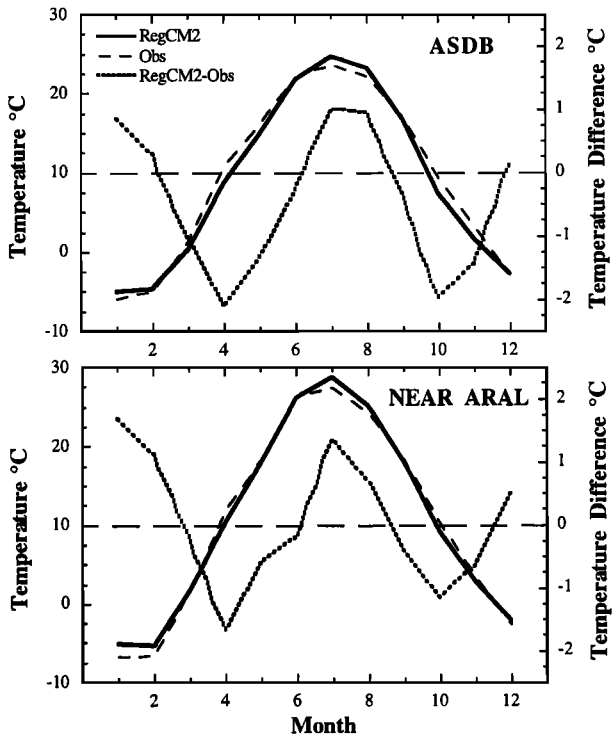

Figure 4. Mean annual cycle of RegCM2 2 m air temperature (solid), CAC air temperature (dashed), and RegCM2-CAC temperature difference (dotted). Top shows average values for the Aral Sea drainage basin, and bottom shows values for the near-Aral region.

temperatures are interpolated across the sea from the shorelines.

To compare simulated and observed values of 2 m air temperature averaged for the near-Aral region and the ASDB, we calculate means only over model grid cells in which meteorological stations exist (Table 2). In both areas, the simulated and observed mean annual temperatures are within 0.3°C. The close match for the ASDB only exists after the adjustment for model-observation elevation differences is completed (Table 2). Larger biases exist when simulated and observed values are compared on a monthly or seasonal timescale (Table 2, Figure 4). The shape of the annual cycle of monthly temperature biases is similar in both areas: biases are more positive in the winter and summer and more negative in the spring and fall (Figure 4). The most negative biases (-2°C) occur in April and October, the months when the rate of temperature change is greatest. This indicates that the model temperatures warm too slowly in the spring and cool too quickly in the fall. This could negatively impact the accuracy of simulated SSTs in these seasons.

In both the near Aral region and the ASDB, simulated temperatures are higher than observed temperatures by ~1°C in July and August. One possible explanation for this bias is that the convective cloud liquid water content prescribed in the model is too low. To test this hypothesis, we completed a 7-month-long integration (May-November 1989) with an increased value for the liquid water content of convective clouds. The resulting optically thicker convective clouds lowered model 2 m air temperatures by ~0.8°C in July and August, reducing the warm bias between simulated and

Table 2. Simulated and Observed 2m Air Temperature Averaged by Season

	DJF	MAM	JJA	SON	Annual
			Aral Sea Drainage Basin		
Number of Stations= 123					
model: grid cells with obs only	-4.6	7.5	22 8	8.4	8.3
observations (without correction)	-4.9 (-3.1)	9.0 (10.8)	22.3 (24.1)	9.1 (10.9)	8.6 (10.4)
model-obs (without correction)	0.3 (-1 5)	-1.5 (-3 3)	0.5 (-1.3)	-0.7 (-2.5)	-0.3 (-2.1)
			Near Aral		
Number of Stations= 51					
model: grid cells with obs only	-4.1	10.1	26.9	10.2	10.8
observations	-5.2	10.9	26.3	10.2	10.5
model-obs	1.1	-0.8	0.6	0.0	0.3

Observed values without the correction for elevation are in parentheses for the Aral Sea drainage basin. The temperature correction in the Aral Sea drainage basin is -1.8°C. The correction for the near-Aral region is <0.1°C, so it is not included. Units are in degrees Celsius.

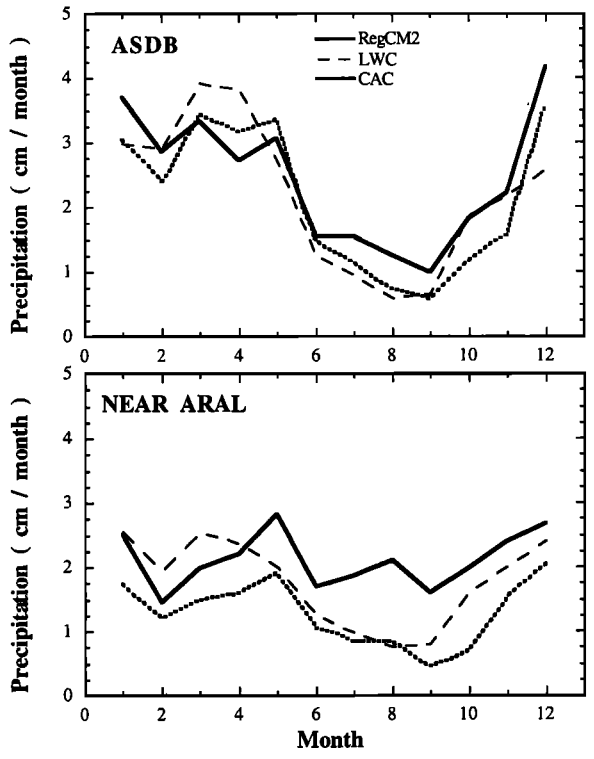

Figure 5. Mean annual cycle of RegCM2 (solid), CAC (dotted), and Legates and Willmott Climatology (LWC) precipitation (dashed). Top shows average values for the Aral Sea drainage basin, and bottom shows values for the near-Aral region.

observed values to near zero. Difference in other months were less than 0.5°C.

4.2. Precipitation

Here we compare the simulated and observed annual cycles of precipitation for the near-Aral region and the ASDB. We calculate means only over model grid cells in which CAC meteorological stations with acceptable precipitation records exist (Figure 5, Table 3). We also show the LWC precipitation averaged for the entire near-Aral region and the ASDB. Compared to the CAC data averaged over the same 5 year interval, RegCM2 simulates the shape of the annual cycle of precipitation well in both areas. Throughout the ASDB, the amplitude of the annual cycle and the timing of the summer minimum and December maximum are simulated well by the model. However, there is no simulated peak during spring, as is the case in the observations. In the near Aral region, RegCM2 accurately simulates the timing of the precipitation peaks in December-January and May. The annual cycles in the Legates and Willmott climatology are similar to those found in the CAC data set.

Although the model simulates the shape of the annual cycle well in both areas, simulated precipitation values are greater than those found in the CAC data set (Figure 5). To estimate how much of this difference is due to the undercatch of rain gauges, we add the spatially varying monthly precipitation correction from the LWC to the CAC data (Table 3). Actual precipitation amounts probably fall between the observed and the observed plus corrected values. The simulated precipitation is within ±10% of the range bounded by the observed and the observed plus corrected values during winter

Table 3. Simulated and Observed Precipitation Averaged for the ASDB and the near-Aral Region

	DJF	MAM	JJA	SON	Annual
			Aral Sea Drainage Basin		
Number of stations= 32					
model: cells with obs only	3.57	3.04	1.44	1.66	2.43
observations (corrected)	3.00 (3.77)	3.32 (3.87)	1.12 (1.23)	1.09 (1.38)	2.13 (2.56)
percent difference (corrected)	16 (-6)	-9 (-27)	23 (15)	34 (17)	12 (-5)
			Near Aral		
Number of stations= 9					
model: cells with obs only	2.21	2.33	1.89	1.99	2.10
observations (corrected)	1.66 (2.66)	1.65 (2.26)	0.91 (1.07)	0.90 (1.28)	1.28 (1.82)
percent difference (corrected)	25 (-20)	29 (3)	52 (43)	55 (36)	39 (14)

Observed (CAC) values, which include the Legates and Willmott correction, are in parentheses. Units are cm/month. Percent difference is calculated as (model-obs)/model.

and spring, in both the ASDB and the near-Aral region. However, simulated precipitation is too high during summer and fall in both areas. We address the impacts of these precipitation overestimates on the water balance of the Aral in the next section.

5. Simulated and Observed Aral Sea Hydrology

5.1. Aral Sea Surface Temperatures

We evaluate how well the coupled RegCM2-lake model simulates Aral SSTs for two reasons. First, SSTs directly influence the rate of evaporation and therefore the water balance of the sea. The evaporation rate is controlled by the difference between the specific humidity of the air and the saturation specific humidity of the water surface (equation (2)), the latter being a function of surface temperature only. The comparison is also useful to assess how well the coupled model represents lake-atmosphere interactions. SSTs directly influence all components of the surface energy balance except shortwave radiation. At the same time, the surface energy balance controls SSTs. If substantial differences exist between modeled and observed SSTs, then the fluxes of heat and moisture between the lake surface and the atmosphere are likely to be incorrect. In particular, the partitioning between sensible and latent heating may be poorly simulated.

The coupled RegCM2-lake model does an excellent job of simulating Aral SSTs compared to the limited set of in situ SST measurements (Figure 6). In this comparison we temporally match each in situ measurement with the simulated SST from the corresponding date and time, within 30 min. In addition, we bilinearly interpolate between the four closest model grid points to estimate the simulated temperature at the location where the measurement was taken. The mean difference between model and in situ SSTs is 0.05°C, with a standard deviation of 0.9°C. The limited scatter between simulated and observed SSTs is surprising, considering that we are comparing observations from a single point with simulated values interpolated between four 50 km^2 grid cells (Figure 6). The largest model biases exist for SSTs of ~25°C, when simulated values are up to 2.5°C warmer than the corresponding in situ observations. It is difficult to evaluate the significance of this bias because of the limited number of in situ measurements.

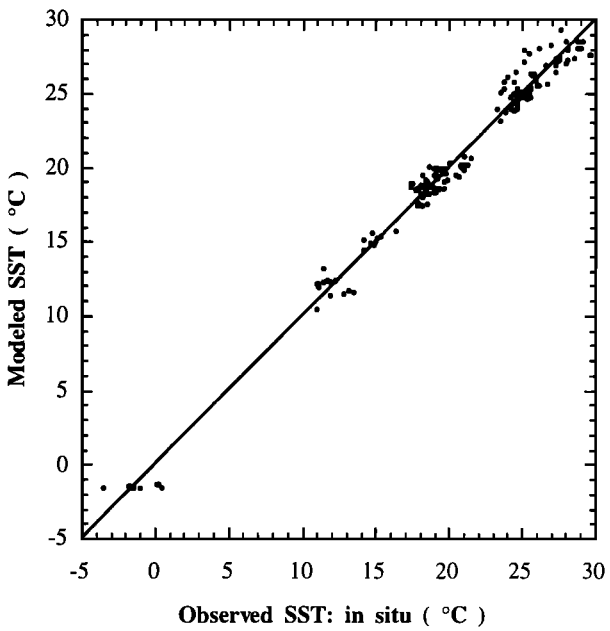

Figure 6. Comparison between modeled and in situ observations of Aral Sea surface temperatures. Solid line shows 1:1 relationship.

To assess the accuracy of the simulated SSTs more fully, we compare the modeled SSTs to the MCSST satellite observations, both averaged over the entire Aral Sea and on a point-by-point basis. We match each 8 day averaged MCSST observation with the corresponding period from the simulation, and the model values are binned into day and night categories to match the observations. For the point comparison, we bilinearly interpolate the simulated SSTs from the four closest model grid cells to the center of each MCSST grid point.

The simulated SSTs closely match the corresponding satellite-derived values, on both a point-by-point basis and averaged for the entire sea (Figure 7). This accurate simulation of SSTs is a substantial improvement over previous efforts with earlier versions of the RegCM2-lake modeling system [e.g., *Bates et al.*, 1995]. The mean difference between modeled and satellite-derived SSTs is -0.58°C during the day and -0.15°C at night. As discussed above, there is a cold bias in the MCSST data of ~0.4°C, compared to buoy measurements. Therefore, on average, the simulated SSTs are too cool by ~1.0°C during the day and ~0.5°C at night. This bias is not constant throughout the year. Compared to the MCSST data, the simulated temperatures are ~2°C too cool during spring and early summer (Figures 8 and 9). Daytime simulated SSTs are also too cool during fall, but the difference is not so large.

The cold model bias during spring may be the result of differences in how the simulated and observed SSTs are calculated. The model value for any 8 day period includes SSTs from both cloudy and clear-sky conditions, whereas the MCSST value only includes temperature measurements under relatively cloud-free skies. This difference results in satellite SSTs that are warmer than model SSTs when the net radiative cloud forcing at the surface is negative, which should be the case over the Aral Sea during spring. These differences should be less important in other seasons, because cloud cover is limited during summer and fall and the net radiative effect of clouds is negligible at this latitude during winter. An alternative explanation for the cold bias in the model during spring is that the simulated SSTs are actually too low, because the RegCM2 surface air temperatures are too low at this time of year (Figure 4). The annual cycles of model-observed differences in air temperature and Aral SST are roughly similar; both simulated quantities are too cool during the spring and fall and too warm in the winter and summer (Figures 4 and 9). Because the SST and domain-wide air temperature biases match, it seems likely that the SST errors are due to problems in the RegCM2 atmospheric inputs to the lake model and not in the representation of lake processes.

5.2 Ice Fraction and Thickness

Like surface temperature, the fraction of ice cover strongly influences the water and surface energy balances of the Aral Sea. For example, evaporation from ice is typically slower than from open water because the ice surface temperature, and

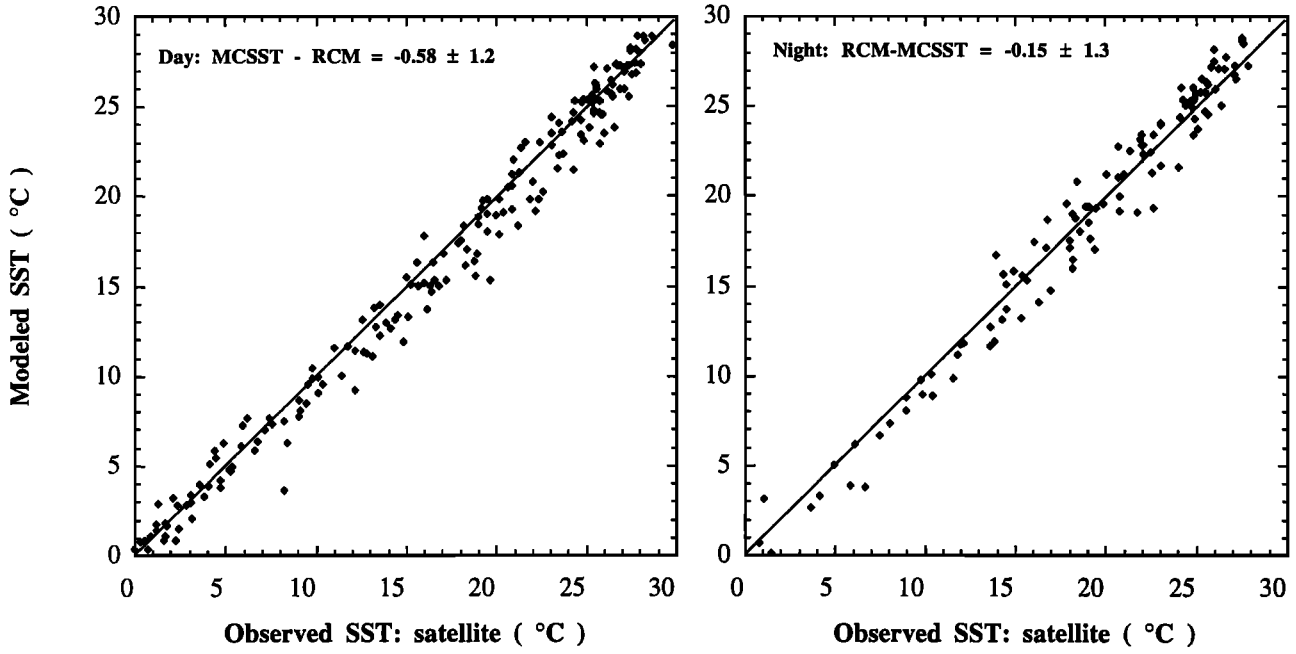

Figure 7. Comparison between modeled and multi channel sea surface temperature (MCSST) observations of Aral Sea surface temperatures, averaged over 8 day windows. Larger dots represent full sea-averaged values. Points represent individual MCSST measurements and corresponding simulated values. Left panel shows daytime simulated and observed SSTs and right panel shows nighttime values. Solid line shows 1:1 relationship. The mean difference (model minus observation) and standard deviation is shown for each plot.

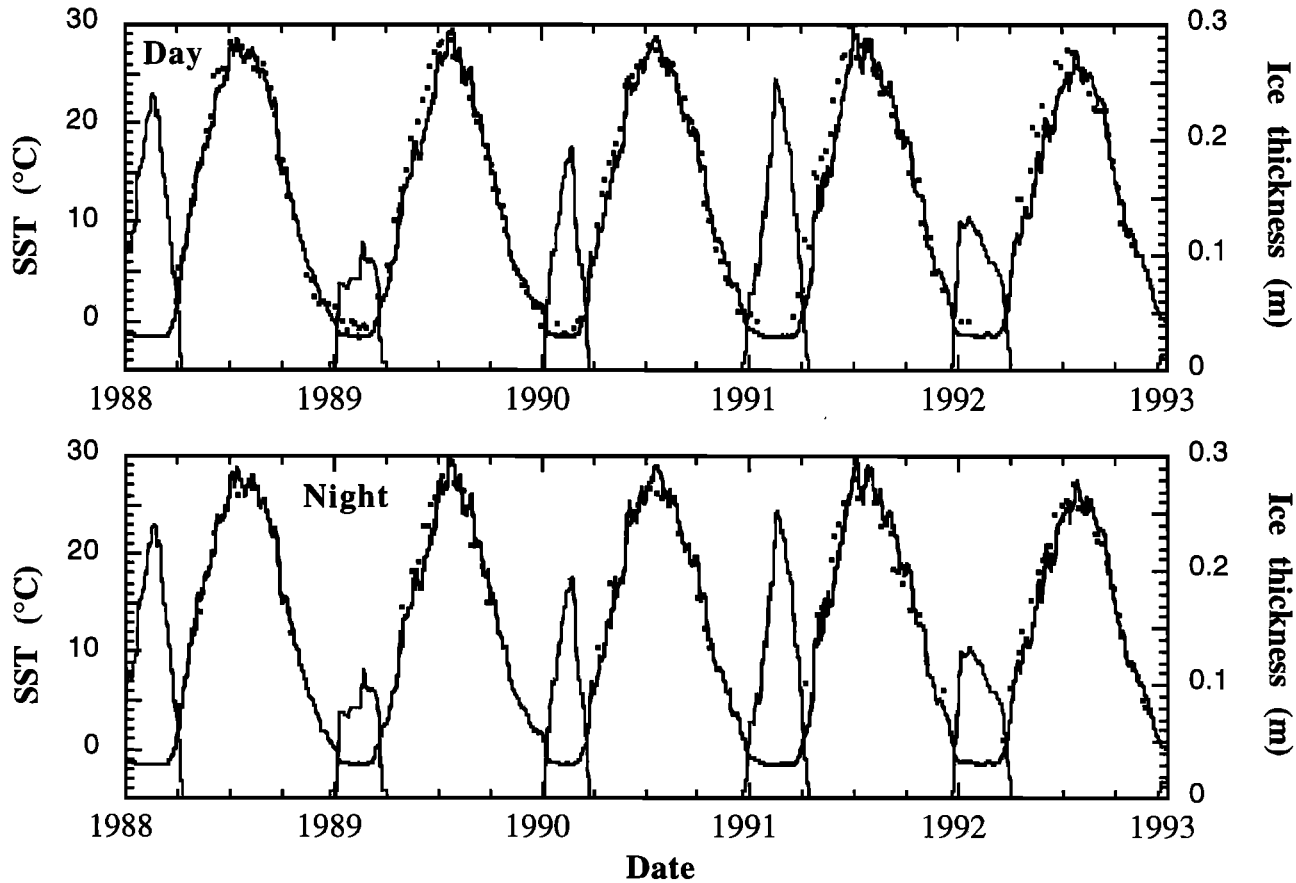

Figure 8. Time series of simulated (thick solid line) and MCSST observed (points) sea- averaged SSTs, for nighttime (top) and daytime (bottom) values. Simulated values are daily averages, and MCSST values are 8 day averages. Simulated ice thickness averaged for the entire Aral Sea is shown by the light solid line. The tick marks on the x axis show the start of January (at the year label), April, June, and October.

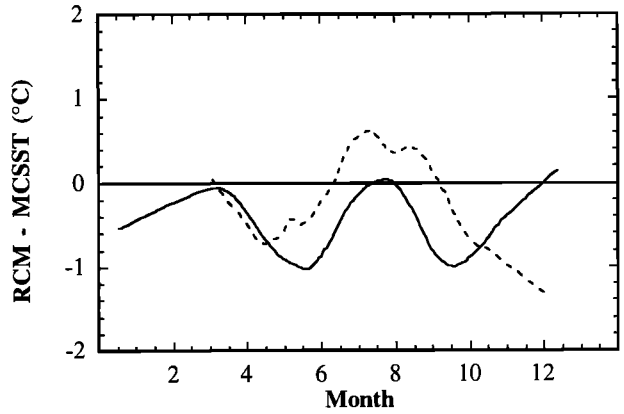

Figure 9. Mean difference between simulated Regional Climate Model (RCM) and MCSST observed 8-day averaged SSTs, plotted by month. Solid line shows daytime difference and dashed shows nighttime.

therefore the surface saturation specific humidity (equation (2)), is frequently lower than that of water. Ice thickness is also important because it controls the flux of sensible heat between the atmosphere and water column. As ice data for the Aral Sea is limited, we make only a first order assessment of the simulated ice cover.

Aral Sea ice fraction data are not available for the period 1988-1992. However, decadal averages for the 1950s through 1970s and a 5 year average for the period 1981-1985 do exist. The ice fraction data were collected from airplanes and satellites and is archived as 10 day averaged values for the entire sea [*Bortnik*, 1990]. Averaged over the period of simulation, the modeled ice fraction is similar to the observed values between January 1 and mid-March (Figure 10). However, modeled and observed values of ice fraction differ before and after this period. As the simulated onset of freezing is ~10 days later than observed, the modeled ice fraction is less than observed throughout December. A greater difference exists during spring, when the simulated ice fraction decreases faster than in the observations. The simulated melting is completed ~15 days earlier than observed between the 1950s and the 1970s and about 5 days earlier than in the first half of the 1980s.

The salinity and depth of the Aral Sea changed dramatically between the 1950's and the period represented by our simulation. Because these characteristics strongly influence ice formation, it is likely that there have also been changes in ice fraction. Therefore it is not possible to assess whether the modeled-observed differences in ice fraction indicate model errors or actual changes in ice fraction associated with desiccation. In addition, decadal variability introduces uncertainty into this comparison. Overall, it appears that the model is simulating ice fraction well, particularly during the middle of the winter. The onset of freezing and completion of melting may be poorly timed, but this cannot be confirmed with the available data.

A time series of simulated Aral Sea ice thickness shows substantial interannual variability in maximum values (Figure 8). For example, the peak value in 1991 is ~0.25 m whereas the peak value in 1989 is only 0.1 m. For the period 1960-1980, point measurements of midwinter ice thickness in the Aral vary from < 0.1 m to 0.6 m, with an average of ~0.4 m [*Bortnik*, 1990]. Again, it is difficult to compare the model output with observations because of the different periods represented by the simulation and measurements and the comparison of sea-averaged values and point measurements. If we weight the ice thickness values in Figure 8 by the simulated ice fraction, the modeled ice thickness, where ice exists, is 0.2 - 0.3 m in midwinter, which is noticeably lower than the observed values. The simulated ice fraction may be decreasing too rapidly in the spring because the ice is not growing thick enough during winter.

5.3. Precipitation Minus Evaporation

The simulated and observed monthly values of P-E are similar between 1988 and 1992 (Figure 11). In nearly all months, both modeled and observed P-E values are negative

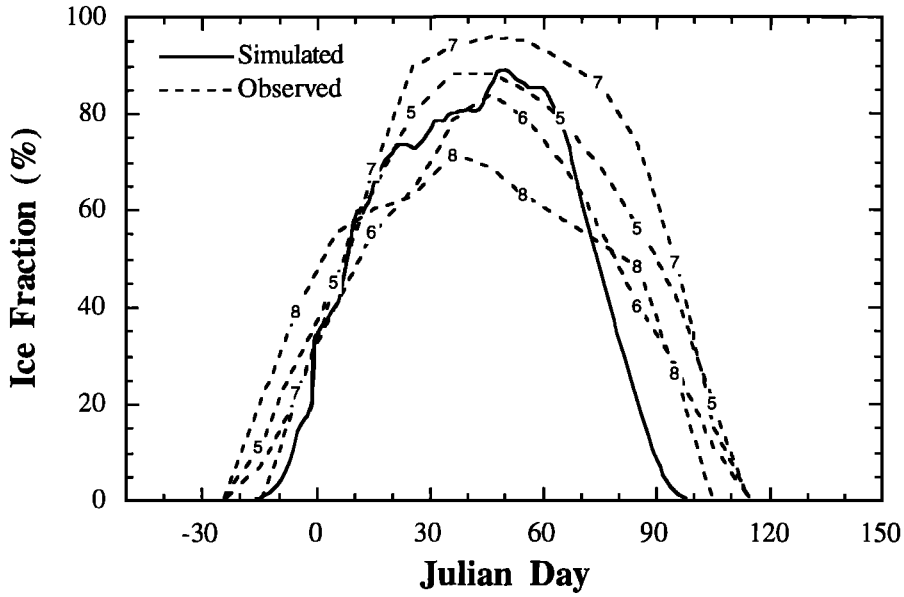

Figure 10. Simulated (solid) and observed (dashed) fraction of Aral Sea covered by lake ice, plotted by Julian day. Modeled values are averaged over period of simulation. Each observed line represents a different decadal average: 5 is 1951-1960; 6 is 1961-1970; 7 is 1971-1980; and 8 is 1981-1985.

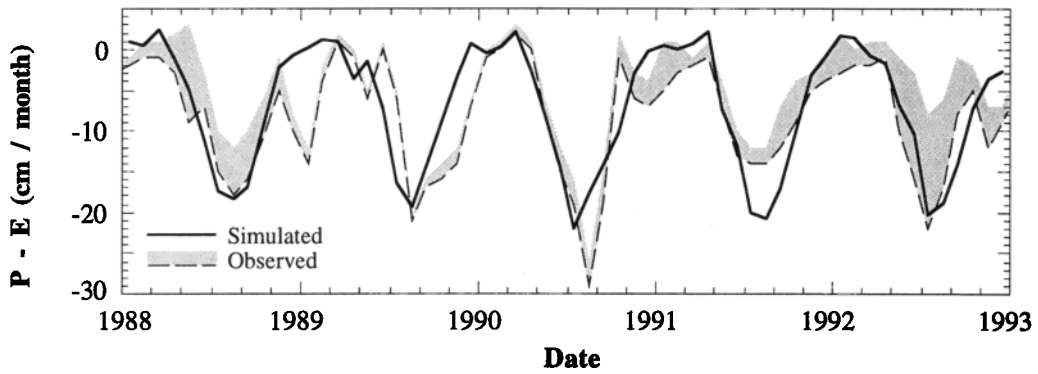

Figure 11. Time series of simulated (solid) and observed monthly precipitation minus evaporation (P-*E*) over the Aral Sea in cm/month. Dashed line shows observed minimum estimate. Shaded region extends from minimum to maximum observed estimate.

because evaporation from the Aral Sea greatly exceeds precipitation on the lake surface. Integrated over the 5 years, the simulated P-E falls between the minimum and the maximum estimates from the observations (Table 4). Whereas the monthly P-E time series are similar, there are many months in which the simulated value deviates from the observed estimate. In some cases these differences are the result of data problems. For example, the observed P-E in August 1990 is -28 cm/month, which is the lowest value in the 5 year record (Figure 11). P-E then increases rapidly to the highest October value. This large P-E fluctuation between August and October 1990 is likely the result of a sea level measurement error, as discussed in section 3.

To avoid the uncertainty in the observations at the monthly timescale, we calculate an average P-E annual cycle for the period 1988-1992. In addition, we separate the precipitation and evaporation components of the P-E observations. We use the LWC annual cycle of precipitation from the near-Aral region (Figure 5) as a proxy for on-lake precipitation. This is probably an accurate estimate because lake effect precipitation from the Aral is minimal [*Lydolph*, 1977]. The simulated and observed annual cycles of precipitation and evaporation for the Aral Sea are shown in Figure 12. Only a small fraction of the Aral Sea P-E budget is due to precipitation on the lake surface (Figure 12 and Table 4). Precipitation is only 20% of evaporation averaged annually and only 5-10% during the summer months. Because of this, the overprediction of precipitation in the near Aral region (Figure 6) has a negligible impact on the simulated hydrologic budget of the sea. It is more critical that the coupled model simulates well the magnitude and annual cycle of evaporation, as this is a much larger component of the Aral Sea hydrologic budget.

Integrated over the annual cycle, the simulated annual evaporation is intermediate between the maximum and the minimum observed estimates (Table 4). However, important differences between simulated and observed values exist in particular months (Figure 12). The simulated evaporation is greater than observed between June and September and less than observed between November and March. This wintertime difference is not uniform in all years between 1988 and 1992 (Figure 11). In each year, the annual P-E minimum occurs in midsummer in both the simulated and the observed records (Figure 11). In the observations, a secondary minimum exists during some winters: in 1989, 1991, and at the end of 1992. These observed wintertime peaks in evaporation probably occur during relatively warm winters when ice cover is limited. These secondary P-E minima are absent in the simulated time series (Figure 11). It is possible that the model is not sensitive enough to interannual variability of wintertime temperatures, and therefore the simulated ice fraction is too high during the winters with high evaporation. The sea-averaged ice thickness is lowest during 1989 (Figure 8) which coincides with the greatest observed wintertime P-E minimum (Figure 11). This suggests that the model does respond to the year-to-year changes in forcing; however, the model response may not be large enough.

As discussed above, RegCM2 surface air temperatures are warmer than observed temperatures by ~1°C during summer, probably because the prescribed liquid water content of convective clouds was too low. This same model shortcoming

Table 4. Simulated and Observed Components of the Aral Sea Water Balence

	Precipitation (cm/yr)	Evaporation (cm/yr)	P-E (cm/yr)	Runoff (km^3/yr)
Model	25	108	-83	162
Observations (minimun)	21	122	-100	~110
Observations (maximum)	21	79	-58	

Precipitation, evaporation, and P-E are calculated over the Aral Sea only, except for observed precipitation, which is the "near-Aral" region average from the LWC.

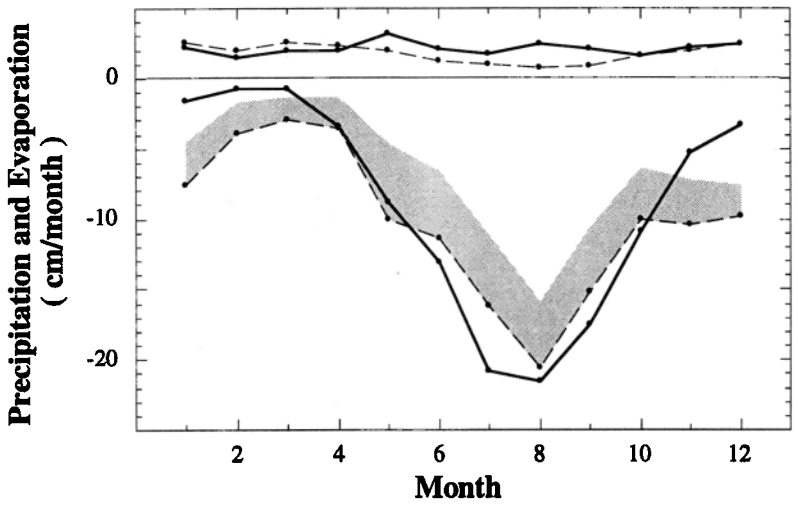

Figure 12. Five year averaged annual cycle of precipitation (positive values) and evaporation (negative values) for the Aral Sea. Simulated values are shown with solid lines, observed with dashed. Observed precipitation is LWC average for the near-Aral region. Shaded region extends from minimum (dashed) to maximum observed estimate of evaporation.

may be responsible for the overestimate of summertime evaporation (Figure 11). During summer, clouds that are optically too thin would raise the lake surface temperature, and therefore evaporation, by increasing the surface incident shortwave radiation. In the 7 month (May-November 1989) simulation with optically thicker convective clouds (discussed above), the simulated evaporation decreased by ~1.5 cm in June, August, and September and by 2.5 cm in July. These changes eliminate the positive evaporation bias in the model, except in July when the simulated evaporation is still too high by 2-3 cm/month.

5.4. Runoff From Mountains

The remaining component of the Aral Sea hydrologic budget is runoff from the Amu Darya and Syr Darya. We do not compare the simulated annual cycle of runoff with observations because this would require a stream-routing scheme. Instead, we assess if the total annual runoff simulated by RegCM2 is in agreement with observations. Prior to 1960, ~60 km^3/yr of runoff reached the Aral Sea. This is a minimum estimate for the volume of runoff that would reach the Aral under natural conditions, because a substantial amount of Amu and Syr Darya water was lost to irrigation and subsequent evaporation at this time. In the 1980s the consumptive loss of river water in the ASDB to irrigation and industry is estimated to have been ~85 km^3/yr [*Micklin*, 1988]. Approximately 15 km^3/yr of water flowed into the Aral during this period, except in dry years. This suggests that runoff to the Aral under natural (human free) conditions is ~100 km^3/year (Table 4).

In BATS, stream runoff is generated by the combination of surface runoff and soil drainage. Averaged over the 5 year simulation, these two sources produce 162 km^3/yr of "runoff" throughout the ASDB defined in Figure 1, which is substantially higher than our estimate of runoff to the Aral Sea under natural conditions (Table 4). The simulated runoff for the entire ASDB should be higher than the observed amount for two reasons: (1) between the runoff source and the Aral Sea, actual river water is lost by evaporation from wetlands and by infiltration to groundwater; and (2) runoff generated throughout much of the low elevation portion of the ASDB (as defined in Figure 1) does not reach the sea but instead collects in ephemeral lakes and eventually evaporates. On the basis of our limited comparison, RegCM2 produces a reasonable amount of runoff averaged over the entire year.

6. Are Lake-Atmosphere Interactions Important?

We have shown that the coupled RegCM2-lake model accurately simulates the present-day water balance of the Aral Sea. In addition, the model closely reproduces air temperature and Aral Sea surface temperatures. Although ice data are limited, the simulated ice fraction and thickness appear reasonable. Does the coupled model successfully reproduce these climatic and hydrologic features because lake-atmosphere interactions are explicitly represented? Or would the model results match observed values as closely even if feedbacks between the lake and the atmosphere were not included? If interactions between the Aral Sea and the atmosphere are weak, the coupled model approach may be unnecessary, and a stand-alone lake model would be sufficient to examine the hydrologic response of the Aral Sea to various forcings.

6.1. Stand-Alone Lake Model Experiments

To evaluate if lake-atmosphere interactions had a strong influence on the control simulation described above, we compare the water balance, SSTs, and lake ice from two stand-alone lake model experiments. In the first experiment ("wet") we force the lake model with meteorological inputs that include the effects of interactions between the Aral Sea and the atmosphere. These inputs are derived from the coupled-model control simulation described above. In the second simulation ("dry") we use meteorological inputs derived from the RegCM2 no-lake simulation, in which the Aral Sea was replaced by desert (described in section 2). In the dry case, the influence of lake-atmosphere interactions is absent in the lake model inputs, because the Aral Sea did not exist in the RegCM2 simulation from which the input data set was derived.

Differences between the results from the wet and dry experiments illustrate how lake-atmosphere interactions affect the simulated hydrology of the Aral Sea system.

In the coupled-model control experiment, the meteorological inputs passed from RegCM2 to the lake model were saved every 30 min. However, in the no-lake RegCM2 simulation, the lake model input variables were not saved at this same frequency. We avoid problems associated with variable input frequency by using an identical method to construct the wet and dry input datasets from the control and no-lake RegCM2 output. We combine 6-hourly values of air temperature, specific humidity, and wind speed from the lowest model level (~40 m) with hourly surface pressure, precipitation, surface incident shortwave, and downward longwave radiation. The only difference in lake model inputs between the wet stand-alone and coupled-model experiments is that the wet inputs exhibit less variability on timescales shorter than 6 hours. This difference has a negligible impact on the wet simulation. The time-varying evaporation, SSTs, and lake ice simulated in the "wet" and coupled-model experiments are nearly identical. Therefore, the effects of lake-atmosphere interactions on Aral Sea hydrology in the coupled-model simulation are duplicated in the wet stand-alone experiment.

Using the wet and dry meteorological inputs, we integrate the stand-alone lake model for the same 5.5 year period that was covered in the coupled-model and no-lake RegCM2 simulations. The depth, salinity, and initial conditions are the same in the wet and dry cases and match those used in the coupled simulation. The stand-alone lake model is exactly the same as that used in the coupled-model experiment.

6.2. Meteorological Inputs

Differences between wet and dry meteorological inputs are entirely the result of replacing the Aral Sea with desert in the no-lake RegCM2 simulation, as no other differences exist between the two model integrations from which the inputs were derived. Replacing the Aral Sea with desert has a large effect on most of the meteorological variables which are input to the lake model (Figure 13). Compared to the coupled-model control simulation, air temperatures from the no-lake experiment are warmer by up to 2.5°C between February and September and cooler by up to 2°C during the remaining fall and winter months (Figure 13a). These air temperature differences are primarily the result of changes in surface temperature associated with replacing the Aral Sea by desert in the no-lake simulation. Desert land surface temperatures are warmer than Aral SSTs during summer and cooler during winter, except when lake ice is present on the Aral.

The change in specific humidity between the coupled the and no-lake RegCM2 simulations is the most substantial among the lake model inputs. Specific humidity at the lowest model level is reduced by ~50% in the no-lake case because evaporation from the desert land surface is extremely limited compared to that from the Aral Sea (Figure 13b). The most extreme difference is in July when evaporation from the Aral Sea is at a maximum (Figure 12). Differences in wind speed are not large between the simulations (Figure 13c). The greatest difference is during fall and winter, when coupled model wind speeds are greater by ~1 m/s. This corresponds to the time of year when the horizontal air temperature gradient between the Aral Sea and the adjacent desert is relatively high.

In the coupled simulation, surface incident shortwave radiation is slightly reduced throughout most of the year, because evaporation from the Aral Sea increases cloud cover locally (Figure 13d). The reverse is true during February and March, when incident shortwave is greater in the coupled simulation than in the no-lake case. During spring the relatively cool water surface of the Great Lakes results in locally descending air and reduced clouds [*Changnon and Jones*, 1972]. A similar process is likely responsible for the shortwave reduction in our simulation. The downward longwave radiation is substantially greater in the coupled model simulation, particularly in the fall and winter (Figure 13e).

6.3. The Simulated Effects of Lake-Atmosphere Interactions

Annually averaged, on-lake precipitation in the no-lake RegCM2 simulation is only ~1.5 cm less than that in the coupled-model experiment, which is an insignificant change compared to the total water budget of the sea (Table 4). In addition, the shapes of the annual cycle of precipitation in the two simulations are nearly identical (not shown). The small change in precipitation between the RegCM2 experiments with and without the Aral Sea is in agreement with observations that there is little or no-lake effect precipitation associated with the Aral [*Lydolph*, 1977]. Runoff from the entire ASDB is also nearly the same between the two experiments. Most of the simulated runoff is generated in the mountains ~1500 km to the southeast of the Aral (Figure 1), so it is reasonable that precipitation over the mountains and the associated runoff are not altered by the presence of the sea. This differs from the results of *Hostetler et al.* [1994]. In their coupled-model study they found that Pleistocene Lake Bonneville greatly influenced the runoff component of its water budget because the lake drainage basin includes mountains that are within ~100 km of the lake. Because changes in on-sea precipitation and ASDB runoff between the two RegCM2 experiments are insignificant, the representation of lake-atmosphere interactions is not critical for a successful simulation of these two components of the Aral Sea hydrologic budget.

Compared to the wet lake simulation forced by coupled-model inputs, the annual Aral Sea evaporation is greater by ~3 cm in the dry experiment. Again, this change is minor compared to the total water budget of the sea (Table 4). The simulated annual evaporation falls between the minimum and the maximum observed evaporation estimates regardless of whether or not lake-atmosphere interactions are represented in the input data set for the lake model. In contrast, the wet and dry inputs result in substantially different annual evaporation cycles (Figure 14). Compared to the wet case, evaporation in the dry experiment is greater during spring and summer and less during winter. Therefore excluding the influence of lake-atmosphere interactions amplifies the differences between the modeled and the observed evaporation described above. This indicates that interactions between the Aral Sea and the atmosphere influence the simulated hydrology and that explicit representation of these interactions improves the simulation of the Aral Sea hydrologic budget.

Whereas the water balance of the Aral Sea is simulated more accurately with the forcing from the coupled model, it is still simulated reasonably well with the dry no-lake forcing. This

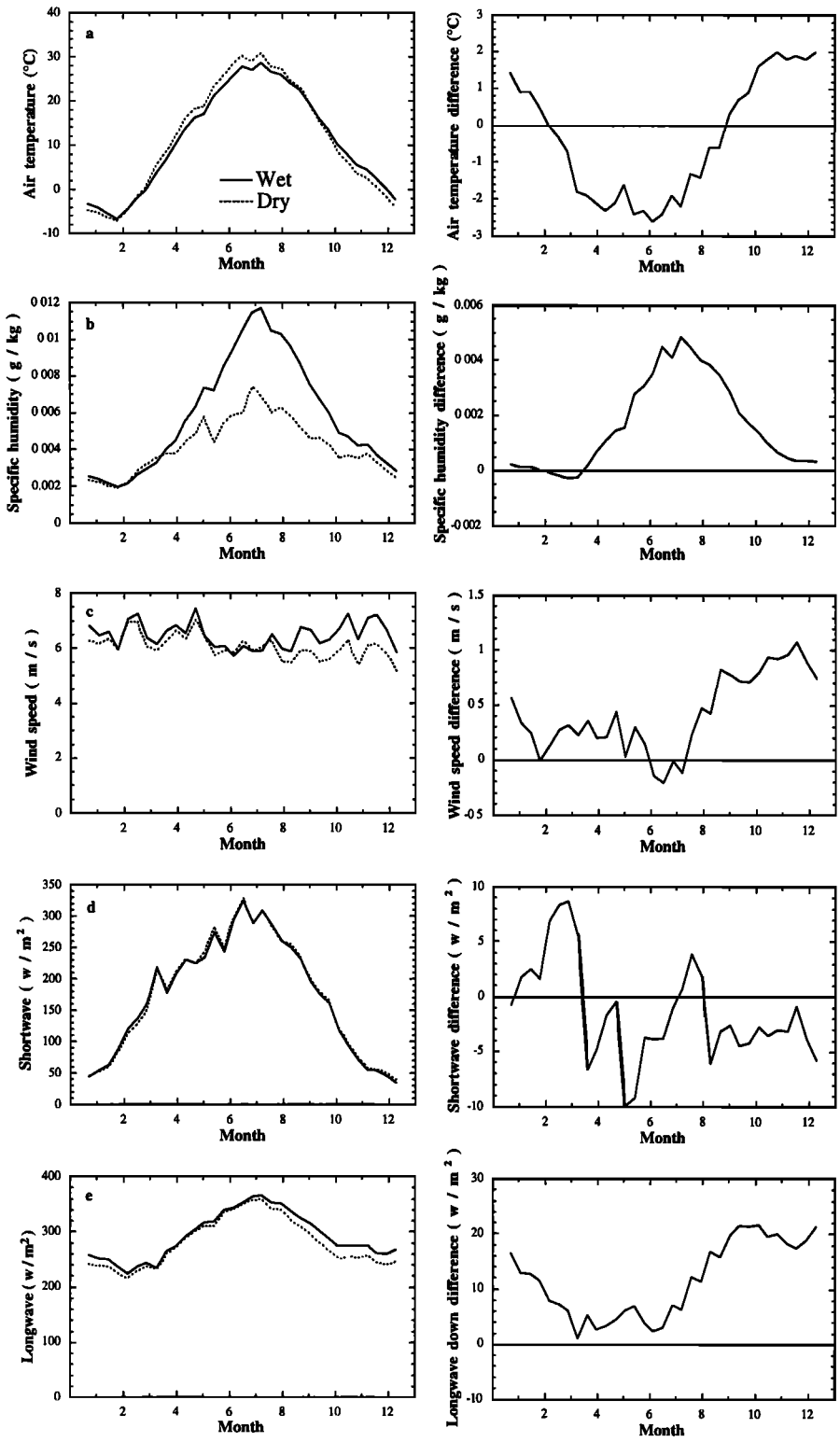

Figure 13. Five year averaged annual cycle of meteorological inputs for wet (solid) and dry (dotted) stand-alone lake model simulations (left) and wet-dry difference (right). Wet inputs are taken from coupled RegCM2-lake model simulation and dry inputs are taken from no-lake RegCM2 simulation. The following inputs are shown: (a) lowest model level air temperature; (b) lowest model level specific humidity; (c) lowest model level wind speed; (d) surface incident shortwave radiation; and (e) downward longwave radiation at the surface.

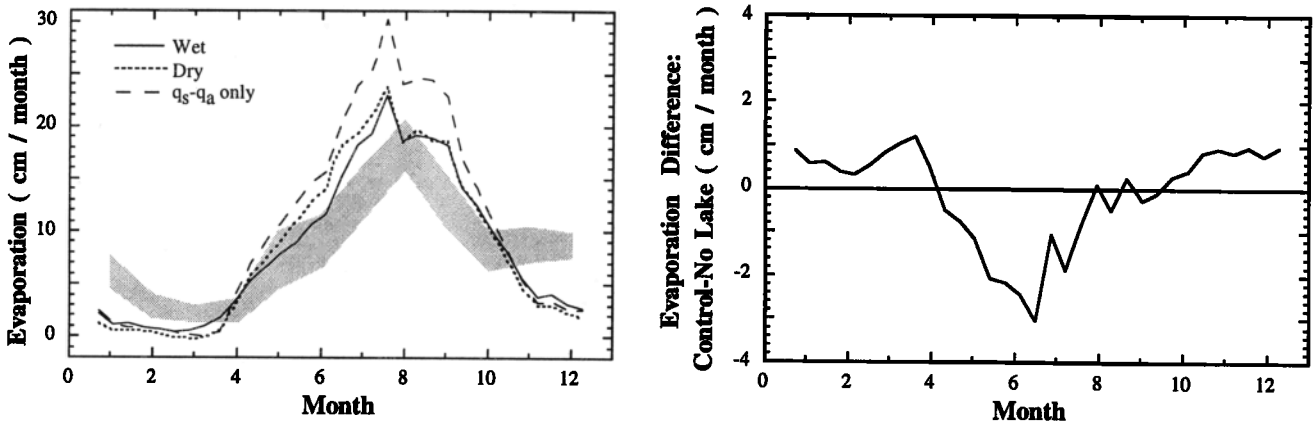

Figure 14. Five year averaged evaporation for wet (solid) and dry (dotted) lake simulations. The shaded region shows the observed evaporation averaged between 1988 and 1992 and extends from the minimum to the maximum estimates of evaporation. The dashed line shows the evaporation that would occur in the dry simulation from changes in $(q_s - q_a)$ only, i.e., without changes in the drag coefficient and wind speed. The difference in evaporation between the wet and the dry simulations is shown on the right

does not necessarily indicate that the model with dry inputs is accurately simulating the processes that control the Aral Sea water balance. However, it is essential to represent accurately these processes when a model is used to project and understand the response of the Aral Sea system to various forcings. As discussed above, one way to check if the important processes are being accurately represented is to examine the simulated SSTs and ice cover, as both of these quantities strongly influence the surface energy balance of the sea.

There are important differences between SSTs in the wet and dry experiments (Figure 15). SSTs are warmer in the wet case, with the greatest differences (~2°C) occurring during the fall and early winter. Relative to the MCSST observations the SSTs are simulated more accurately throughout the year with the wet forcing, except during October and November when SSTs from both simulations are equally close to observed values (Figure 15). These changes in SST are accompanied by changes in the fraction of ice cover (Figure 16). Ice growth begins earlier in the dry experiment because SSTs are lower during the fall and early winter. Whereas the midwinter ice fraction maximum in the wet experiment is only ~80%, the Aral Sea is fully covered by ice for 40 days in the dry case. Again, the results from the wet simulation compare more favorably with observations, as the observed (1951-1985 average) midwinter ice fraction maximum is ~80% (Figure 16) and never reaches 100% in any of the individual decadal averages (Figure 10). Compared to the observations, the duration of ice cover is simulated better in the dry experiment. However, this apparent improvement is the result of two compensating errors: the midwinter ice fraction is too high, and the rate of ice fraction decrease is too fast in the spring compared to the observations.

Changes in SST and ice fraction between the dry and the wet simulations are both the product of and lead to differences in the various components of the surface energy balance between the two experiments (Figure 17). Compared to the wet experiment, evaporation is greater in the dry case between April and September because the specific humidity of the air is lower (Figure 13b). The result is increased latent cooling of the lake surface in the dry experiment (more energy leaving the surface), with a maximum difference of ~25 w/m^2 during midsummer (Figure 17). Between May and August this difference is the dominant surface energy balance change between the two simulations and produces the relatively cool

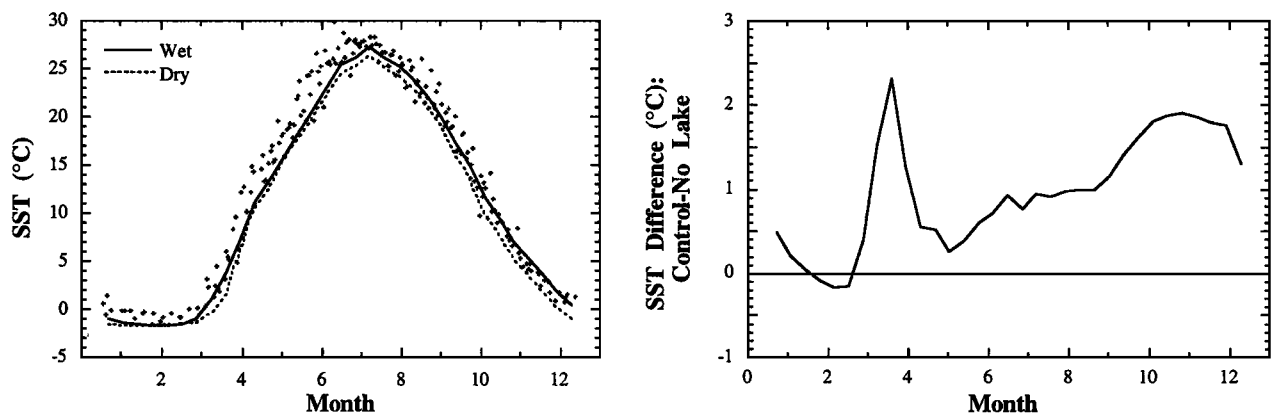

Figure 15. Five year averaged Aral SST for wet (solid) and dry (dotted) lake simulations (left). Dots show MCSST daytime sea-averaged values. Temperature differences between the wet and dry simulation are shown on right.

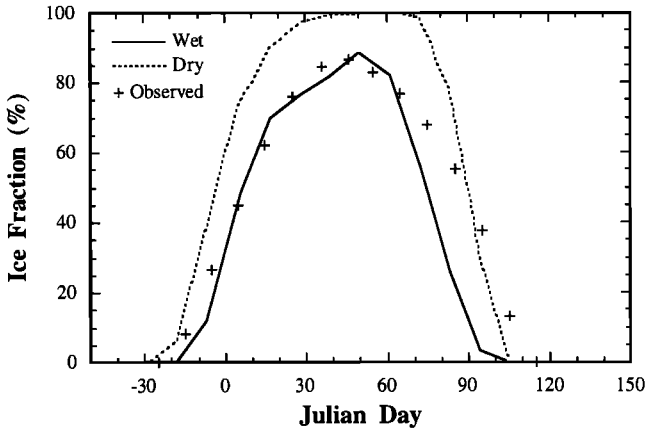

Figure 16. Five year averaged Aral Sea ice fraction for wet (solid) and dry (dotted) lake simulations, plotted by Julian day. The plus symbols show observed ice fraction, averaged over the period 1950-1985.

summertime SSTs in the dry case (Figure 15). The dry experiment SSTs continue to decrease relative to those in the wet experiment between September and December (Figure 15), even though the wet-dry difference in latent heating is opposite in sign of that during summer (Figure 17). During this portion of the year, net longwave radiation is relatively low in the dry case (Figure 17) because the downward longwave radiation from the atmosphere is greatly reduced in the absence of lake-atmosphere interactions (Figure 13e). The large difference between the wet and the dry longwave inputs (~20 w/m^2) is partially offset by the cooler fall SSTs in the dry experiment, which results in a reduction of the longwave radiation emitted from the lake surface.

Sensible heating of the lake surface is greater by up to 20 w/m^2 in the dry experiment (Figure 17). Between February and October, dry experiment SSTs are cooler (Figure 15) and air temperatures are warmer than in the wet case (Figure 13a). This increases the surface-air difference in temperature and the associated sensible heat flux (equation (3)). During the spring and summer the sensible heating of the lake surface is doubled in the dry experiment, and the Bowen ratio is approximately 2 times higher. Although there is only a small difference in the total surface energy balance during summer between the two cases, both the latent and sensible heat fluxes are substantially greater in the dry experiment. This shows that the processes that produce the simulated water balance change dramatically when lake-atmosphere interactions are not represented, even if the final simulated water balance is not very different.

The specific humidity of the air in the dry case is lower than in the wet experiment by ~50% (Figure 13b). Because the evaporation rate increases linearly with the surface-to-air difference in specific humidity (equation (2)), it is surprising that this large change in inputs yields only a 10-15% increase in summertime evaporation (Figure 14). Several factors limit the sensitivity of summertime evaporation to the change in specific humidity. The increased evaporation in the dry case results in cooler SSTs, which decreases the saturation specific humidity of the lake surface and the surface-to-air specific humidity difference. This change is substantial because saturation specific humidity increases nonlinearly with temperature. Even though cooler SSTs offset the decrease in specific humidity of the air, the combined effects of changes in specific humidity and SST in the dry experiment, as represented by (q_S-q_a) in equation (1), would result in larger changes in evaporation than those that actually occurred (Figure 14). This indicates that changes in factors other than (q_S-q_a) must work to reduce evaporation in the dry experiment, relative to the wet case. Changes in wind speed between the two experiments are small and are not the source (Figure 13c). Instead, surface drag coefficients are much reduced in the dry experiment during summer (not shown), which has the effect of lowering evaporation below that resulting from changes in (q_S-q_a) only (Figure 14). Drag coefficients are reduced in the dry case because stability is increased, as SSTs are lower and air temperatures are higher than in the wet experiment.

7. Conclusions

RegCM2 simulates surface air temperature well, including the spatial patterns and annual cycle. However, there is a cold bias of up to 2°C during spring and fall and a lesser warm bias

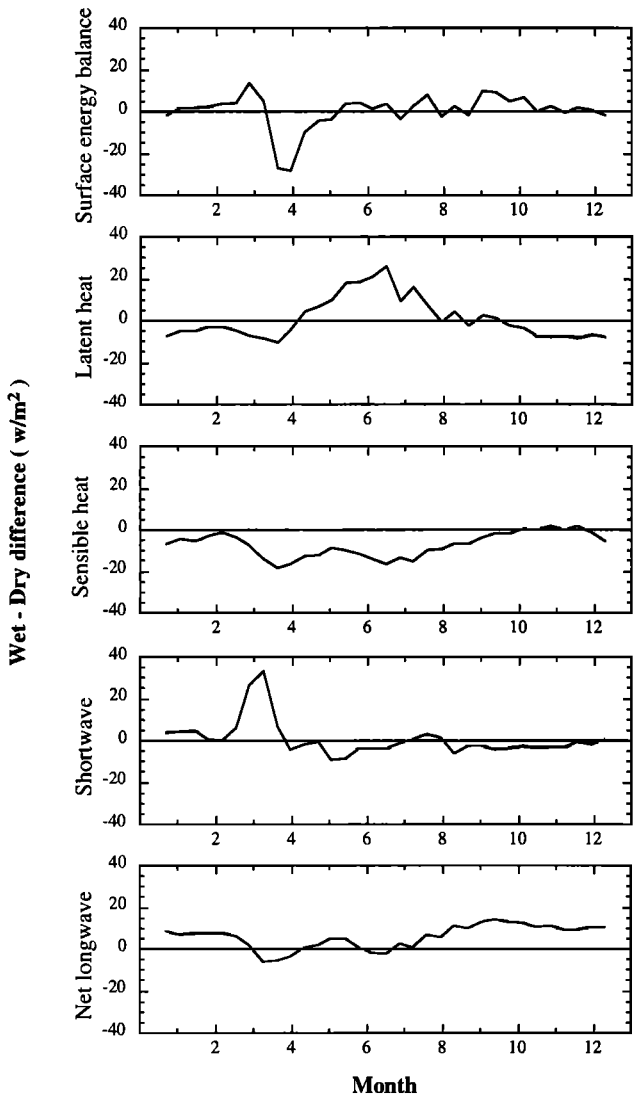

Figure 17. Five year averaged surface energy balance differences between wet and dry stand-alone lake simulations. All plots show wet-dry difference.

during winter and summer, the latter resulting from the convective cloud liquid water content prescribed in the model being too low. The shape of the annual cycle of precipitation is also simulated well, but the magnitude of precipitation is too high during summer and fall. This bias has a negligible impact on the simulated water balance of the Aral Sea because on-lake precipitation is a very small component of the water budget during these seasons. On a yearly basis, RegCM2 produces a reasonable amount of runoff throughout the Aral Sea drainage. Overall the performance of the regional climate model is satisfactory in terms of the inputs to the coupled lake model.

On the basis of comparisons with in situ and satellite observations, the coupled atmosphere-lake model accurately simulates Aral SSTs. This represents a substantial improvement over previous efforts with earlier versions of the RegCM2-lake modeling system. SST biases match the RegCM2 air temperature biases over land throughout the domain: SSTs and air temperatures are too cool in the spring and fall and too warm in the winter and summer. This suggests that SST errors are the result of problems with the regional climate model inputs to the lake model. The coupled model simulates the midwinter ice fraction well, although the onset of ice growth appears too late and the ice melts too rapidly in the spring. As the ice observations are limited and from a different period, it is difficult to draw firm conclusions about model performance.

The annual evaporation simulated by the coupled RegCM2-lake model is intermediate between the maximum and the minimum observed estimates. However, simulated evaporation is greater than observed during summer and less than observed during winter by up to ~4 cm/month. The summertime difference is largely due to the convective cloud problems in RegCM2. Wintertime evaporation is only simulated poorly in the years with relatively high cold season evaporation, as seen in the monthly time series of observed P-E values. The coupled model may overestimate ice cover in these relatively warm years, leading to an underprediction of evaporation.

The coupled RegCM2-lake model simulates well the various components of the Aral Sea hydrologic budget. In addition, the simulated air temperatures, SSTs, and ice cover match observed values closely, suggesting that the processes controlling the Aral Sea surface energy balance are also simulated well. Lake-atmosphere interactions exert a strong influence in this simulation. When these effects are excluded, the simulated Aral Sea hydrology deteriorates in several ways: (1) the simulated annual evaporation cycle does not match observations closely, as the model biases in both summer and winter evaporation increase; (2) differences between simulated and observed SSTs increase; (3) the Aral Sea is completely covered by lake ice for 40 days each winter, which is unrealistic; and (4) the sensible heating of the lake surface is doubled because SSTs are cooler and air temperatures are warmer. These results show that a stand-alone lake model is insufficient to study the effects of climate and hydrologic change on the Aral Sea.

Acknowledgments. This work was funded by NSF ATM-9632304 (to LCS). We thank C. Morrill, G. Hancock, A. Ewing, S. Bucketts, and C Shields for their assistance. In addition, we thank two anonymous reviewers for their helpful comments

References

Anthes, R C. A., E. Y. Hsie, and Y. H Kuo, Description of the Penn State/NCAR mesoscale model version 4 (MM4), *NCAR Tech. Note, NCAR/TN-282*, 66 pp., Natl. Cent. for Atmos Res., Boulder, Colo , 1987.

Bates, G T , S W Hostetler, and F. Giorgi, Two-year simulation of the Great Lakes Region with a coupled modeling system, *Mon. Weather Rev , 123*, 1505-1522, 1995.

Bonan, G. B., Sensitivity of a GCM simulation to inclusion of inland water surfaces, *J. Clim., 8*, 2691-2704, 1995.

Bortnik, B. H., Hydrometeorology and hydrology of the seas of the Soviet Union: The Aral Sea (in Russian), 660 pp , Akademiya Nauk SSSR, Moscow, Russia, 1990.

Briegleb, B. P., Delta-Eddington approximation for solar radiation in the NCAR community climate model, *J Geophys. Res., 97*, 7603-7612, 1992.

Changnon, S. A., and D. M. A. Jones, Review of the influences of the Great Lakes on weather, *Water Resour Res., 8*, 360-371, 1972.

Coe, M T., and G. B. Bonan, Feedbacks between climate and surface water in northern Africa during the middle Holocene, *J. Geophys. Res., 102*, 11,087-11,101, 1997.

Dickinson, D. R , J. H. Yepsen, and J. V. Hales, Saturated vapor pressures over Great Salt Lake brines, *J. Geophys. Res., 70*(2), 500-503, 1965.

Dickinson, R. E., R. M. Errico, F. Giorgi, and G. T. Bates, A regional climate model for the western United States, *Clim. Change, 15*, 383-422, 1989.

Dickinson, R. E., A. Henderson-Sellers, and P J Kennedy, Biosphere-atmosphere transfer scheme (BATS) version 1e as coupled to the NCAR community climate model, *NCAR Tech. Note, NCAR/TN-387+STR*, 72 pp , Natl. Cent for Atmos. Res., Boulder, Colo., 1993.

Gill, A. E , *Atmosphere-Ocean Dynamics*, 662 pp., Academic, San Diego, Calif., 1982.

Giorgi, F., Simulation of regional climate using a limited area model nested in a general circulation model, *J. Clim., 3* , 941-963, 1990.

Giorgi, F., and G. T. Bates, The climatological skill of a regional model over complex terrain, *Mon. Weather Rev., 117*, 2325-2347, 1989

Giorgi, F., and L. O. Mearns, Approaches to the simulation of regional climate change: A review, *Rev. Geophys , 29*(2), 191-216, 1991.

Giorgi, F , and C. Shields, Tests of precipitation parameterizations available in the latest version of the NCAR regional climate model (RegCM) over the continental United States, *J. Geophys. Res* , this issue

Giorgi, F., M. R. Marinucci, and G. T Bates, Development of a second-generation regional climate model (RegCM2), I, Boundary-layer and radiative transfer processes, *Mon. Weather Rev., 121*, 2794-2813, 1993a.

Giorgi, F , M R. Marinucci, and G. T. Bates, Development of a second-generation regional climate model (RegCM2), II, Convective processes and assimilation of lateral boundary conditions, *Mon. Weather Rev , 121*, 2814-2832, 1993b.

Giorgi, F., C. Shields Brodeur, and G. T. Bates, Regional climate change scenarios over the United States produced with a nested regional climate model, *J. Clim ,7*, 375-399, 1994.

Graham, J., Secchi disk observations and extinction coefficients in the central and eastern North Pacific Ocean, *Limnol. and Oceanogr., 11*, 184-190, 1966.

Grell, G. A., Prognostic evaluation of assumptions used by cumulus parameterizations, *Mon. Weather Rev , 121*, 764-787, 1993.

Henderson-Sellers, B , New formulation of eddy diffusion thermocline models, *Appl. Math Model , 9*, 441-446, 1985.

Henderson-Sellers, B., Calculating the surface energy balance for lake and reservoir modeling· A review, *Rev. Geophys., 24*(3), 625-649, 1986.

Hjelmfelt, M. R., Numerical study of the influence of environmental conditions on lake-effect snowstorms over Lake Michigan, *Mon. Weather Rev., 118*, 138-150, 1990.

Holtslag, A. A. M , E. I. F. de Bruin, and H. L. Pan, A high resolution air mass transformation model for short-range weather forecasting, *Mon Weather Rev., 118*, 1561-1575, 1990.

Hostetler, S. W., and P. J. Bartlein, Simulation of lake evaporation with application to modeling lake level variations of Harney-Malheur Lake, Oregon, *Water Resour. Res.*, 26, 2603-2612, 1990.

Hostetler, S. W , and F. Giorgi, Effects of a 2 X CO_2 climate on two large lake systems: Pyramid Lake, Nevada, and Yellowstone Lake, Wyoming, *Global Planet. Change, 10*, 43-54, 1995.

Hostetler, S. W., G. T. Bates, and F. Giorgi, Interactive coupling of a lake thermal model with a regional climate model, *J. Geophys. Res., 98*, 5045-5057, 1993.

Hostetler, S. W., F. Giorgi, G. T. Bates, and P. J. Bartlein, Lake-atmosphere feedbacks associated with Paleolakes Bonneville and Lahontan, *Science, 263*, 665-668, 1994

Jones, R. G., J. M Murphy, and M. Noguer, Simulation of climate change over Europe using a nested regional-climate model, I, Assessment of control climate, including sensitivity to location of lateral boundaries, *Q. J. R. Meteorol Soc., 121*, 1413-1449, 1995

Legates, D. R., and C. J. Willmott, Mean seasonal and spatial variability in gauge-corrected, global precipitation, *Int. J. Climatol., 10*, 111-127, 1990.

Lofgren, B. M., Simulated effects of idealized Laurentian Great Lakes on regional and large-scale climate, *J. Clim., 10*, 2847-2858, 1997.

Lydolph, P. E., *Climates of the Soviet Union*, Elsevier Sci., New York, 1977.

McClain, E. P., Global sea surface temperatures and cloud clearing for aerosol optical depth estimates, *Int. J. Remote Sens., 10*, 767-769, 1989

McClain, E. P., W G. Pichel, and C. C. Walton, Comparative performance of AVHRR-based multichannel sea surface temperatures, *J. Geophys. Res., 90*, 11,587-11,601, 1985.

Micklin, P. P., Desiccation of the Aral Sea: A water management disaster in the Soviet Union, *Science, 241*, 1170-1176, 1988.

Morton, F. I., Evaporation from large deep lakes, *Water Resour. Res., 3*(1), 181-200, 1967.

Patterson, J. C., and P F. Hamblin, Thermal simulation of a lake with winter ice cover, *Limnol. Oceanogr., 33*(3), 323-338, 1988.

Sadov, A.V., and V V. Krasnikov, Detection of foci of subaqueous subsurface water discharge into Aral Sea by remote sensing methods, *Probl. Osvoeniya Pustyn, 1*, 28-36, 1987.

Small, E. E., F. Giorgi, and L. C. Sloan, Regional climate model simulation of precipitation in central Asia: Mean and interannual variability, *J. Geophys. Res.*, this issue.

Trenberth, K. E., Global analyses from ECMWF and atlas of 1000 to 10 mb circulation statistics, *NCAR Tech. Note,_NCAR/TN-373+STR*, 191 pp , Natl. Cent for Atmos Res., Boulder, Colo., 1992.

F. Giorgi, National Center for Atmospheric Research, Boulder, CO 80307.

L. C. Sloan, and E. E. Small, Department of Earth Science, University of California Santa Cruz, 95064. (e-mail: lcsloan@es.ucsc.edu, esmall@es.ucsc.edu)

(Received February 20, 1998; revised June 5, 1998; accepted June 5, 1998.)